Journal Pre-proof

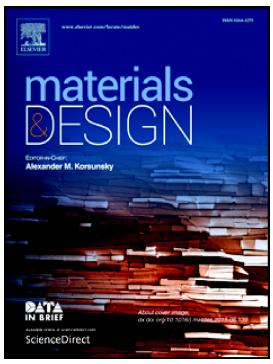

Internal diameter HVOAF thermal spray of carbon nanotubes reinforced WC-Co composite coatings

F. Venturi, S. Kamnis, T. Hussain

PII: S0264-1275(21)00119-2

DOI: https://doi.org/10.1016/j.matdes.2021.109566

Reference: JMADE 109566

To appear in: *Materials & Design*

Received date: 30 November 2020

Revised date: 14 January 2021

Accepted date: 5 February 2021

Please cite this article as: F. Venturi, S. Kamnis and T. Hussain, Internal diameter HVOAF thermal spray of carbon nanotubes reinforced WC-Co composite coatings, *Materials & Design* (2021), https://doi.org/10.1016/j.matdes.2021.109566

This is a PDF file of an article that has undergone enhancements after acceptance, such as the addition of a cover page and metadata, and formatting for readability, but it is not yet the definitive version of record. This version will undergo additional copyediting, typesetting and review before it is published in its final form, but we are providing this version to give early visibility of the article. Please note that, during the production process, errors may be discovered which could affect the content, and all legal disclaimers that apply to the journal pertain.

© 2021 Published by Elsevier.

Journal Pre-proof

Internal diameter HVOAF thermal spray of carbon nanotubes reinforced WC-Co composite coatings

F. Venturi[1], S. Kamnis[2,**] spyros@monitorcoatings.com, T. Hussain[1,*] tanvir.hussain@nottingham.ac.uk

[1]Faculty of Engineering, University of Nottingham, University Park, Nottingham, NG7 2RD, United Kingdom

[2]Castolin Eutectic - Monitor Coatings Ltd, North Shields NE29 8SE, United Kingdom

[*]Corresponding author.

[**]Co-corresponding author.

Abstract

A novel process, relatively fast and scalable compared to existing ones, has been used to incorporate carbon nanotubes (CNT) 0.5 wt. % onto commercial WC-Co thermal spray powder. Nano enabled WC-Co/CNT coatings were obtained by internal diameter HVOAF thermal spray at three different spray powers (48, 41 and 34 kW). A general increase in microhardness and decrease in fracture toughness has been found when adding CNT. Also, carbide retention index upon spray was improved by lowering the process temperature and adding CNT, reaching 99 % in the low power case with CNT. The interplay of these features has shown an overall better wear performance in the medium power case without CNT; in fact, the addition of CNT has improved the wear performance at high power conditions (reduction of coefficient of friction by half) while reducing the wear performance in medium and low power. A tailored choice of CNT concentration can offer enhanced mechanical or tribological properties according to the needs for different applications. This novel process for nanoparticles incorporation opens the way for the production of large batches of readily usable nano-enabled powder.

Keywords

HVOAF thermal spray, internal diameter spray, wear-resistant coatings, WC-Co, carbon nanotubes.

1 - Introduction

The problem of degradation and failure of moving mechanical parts in contact due to friction and wear has been tackled in different ways, including design enhancement, surface modification, lubrication and coating. Coatings are in general a favourable solution for protecting parts not only from friction and wear [1] but also from corrosion [2], erosion [3], thermal shocks [4] and other environmental factors [5]. The application of a coating to mechanical parts is a widespread and convenient manufacture practice as it allows to combine the optimal bulk mechanical properties and cost-efficiency of the part itself with the enhanced surface properties endowed by the coating.

Thermal spray is a well-established coating technique with the capability of coating broad areas in little time with high-hardness wear-resistant coatings [6] but, as most line-of-sight techniques, it encounters limitations when spraying parts with complex geometries or narrow apertures. In fact, traditional thermal spray cannot deposit coatings in the inner surface of narrow parts, with the exception of the more exterior sections if the thermal spray jet is directed towards the target at an angle. This can cause a modification of coating properties such as hardness and porosity compared to the spray carried out at an optimal incidence angle. Recent technological advances with new compact thermal spray gun designs have allowed internal diameter (ID) spray in narrow apertures such as pipes, engine cylinder bores and hollow parts in general. Most ID thermal spray guns designs involve a right-angle shaped expansion nozzle where the length must be kept at a minimum in order to fit in the narrow aperture [7]. Also, the stand-off distance between the gun exit and the part has to be long enough to provide a proper acceleration and melting of the feedstock in-flight [8] while preventing overheating of the target, additional reasons for the need of gun miniaturisation. Additional challenges in ID spray are the ability to rotate the gun and/or the part to allow even coating deposition, and to provide good removal of oversprayed particles avoiding redeposition inside the narrow part. ID coatings have so far been applied to

internal surfaces as narrow as 70 mm in diameter, without compromising the quality of the coating [9].

The choice of materials to be used as wear-resistant coatings includes mainly cermets [9,10] and often comprises very hard phases like nitrides and carbides such as TiN, TiC, SiC, and WC and a metallic binder. WC is often the best choice among these due to its higher Young's modulus, lower thermal expansion coefficient and hardness stability over a wider range of temperatures [11]. WC usually is sprayed together with Co due to their high wettability; Co acts as a binder yielding a strong bonding to keep together the hard WC phase in forming a hard, wear-resistant coating [12]. This material constitutes one of the industrial gold standards for high wear resistant applications in harsh environments for oil and gas, metallurgy, mining and nuclear industries. Nonetheless, there is an interest in widening the applicability, durability and reliability of WC-Co coatings. Further improvements in wear-resistant coatings have recently been explored by powder densification [13] or by adding small fractions (<5%) of nanofillers such as carbon-based materials as graphene nanoplatelets (GNP) and carbon nanotubes (CNT) [14] or other lamellar materials as WS_2 and MoS_2 as reinforcements phases. These carbon allotrope materials are overall characterised by high Young's modulus [15,16] and/or solid lubricating properties [17] and offer enhanced microhardness [18] and reduced friction properties [19] to the materials they are added to. In particular, CNTs are characterised by a fibre-like morphology which allows them to bend and easily adhere on curved surfaces, making them suitable for incorporation in composite coatings. These nano-enabled materials have the potential of pushing forward the current limitations of wear-resistant coatings, such as durability and friction, by providing novel, enhanced tribomechanical properties [20]. At the same time, there is still a need for developing efficient ways to incorporate CNT into coatings and understanding the interplay between their addition and the spray conditions have on the final coating performance.

In this work, CNTs nanofillers have been added to commercial WC-Co powder using a novel ultrasonication-based setup which provided efficient dispersion of CNTs throughout the surface of the powder particles, with promising scale-up possibility compared to existing jar milling methods [21]. The combination of WC-Co and CNT was sprayed using an ID HVOAF gun at three different spray conditions, where the HVOAF gases total flowrate varied to

provide three different flame powers. The aim of the work is producing wear-resistant coatings with enhanced tribomechanical properties for ID application thanks to the addition of CNT nanofillers. The mechanical, structural and tribology properties of the coatings have been analysed and the influence of the three sets of spray parameters and the addition of CNT has been studied. The proposed mixing setup has the potential to be applicable to many different combinations of nanoparticles and commercial powders.

2 - Material and methods

2.1 - Materials

A commercial WC-Co 83-17 powder (AMPERIT® 526.059, Höganäs, Germany) with nominal particle size of 30/5 µm and multi-walled CNT (abcr, Germany) with 50 nm nominal diameter and 1-2 µm length, were used as powder feedstock. The CNT powder was suspended in deionised water with the addition of 0.1 wt.% Sodium Dodecyl Sulphate and mixed using an ultrasonicator (Fisher Scientific, United Kingdom) for 1 hour. The WC-Co powder was then added to the suspension, with a final CNT concentration of 0.5 wt. % compared to the WC-Co weight. This process can efficiently handle 50 g WC-Co powder per batch, and needs to be repeated to reach the desired amount of feedstock. The mixture was further ultrasonicated for 1 hour; in this part of the process the WC-Co particles come in contact with the suspended CNTs which adhere on their surface in forming the composite particles. The mixture was then dried in an oven overnight at 60 °C and again mixed using a Turbula shaker mixer (WAB, Switzerland) with fixed rotational speed for 10 minutes. The CNT concentration in the final powder is again 0.5 wt. % compared to the WC-Co weight, as there is no loss during this process.

2.2 - Thermal Spray

Three sets of spray flowrate parameters were used in order to obtain three different flame powers, labelled as high power (HP), medium power (MP) and low power (LP). The corresponding normalised flowrate values are presented in Table 1. The various flowrate regimes have an effect on the combustion process inside the HVOAF gun and of particular importance is the air flowrate, which has an effect in lowering the flame temperature since only part of it will actively take part to the combustion process. The different flame power values will increase both the flame temperature and velocity as the power increases: this

has the dual effect of increasing the temperature of the particles but also decreasing their residence time in the flame due to a higher flame velocity. Throughout the paper the aspect of temperature will be mainly considered as it is the major effect of the change in power, but the interplay of higher temperature-shorter residence time is always present and must be kept in mind. The spray setup is the same as described in our previous work [9] with an ID HVOAF gun [22]. The powder was fed using a volumetric disc-based powder feeder, with slight adjustments in RPM and carrier gas flowrate to keep the powder feed rate constant in all runs. The coatings were deposited on AISI 416 stainless steel discs (nominal composition: 12–14% Cr, 1.25% Mn, 0.15% C, 0.15% S, 0.6% Mo, 0.06% P, 1% Si in wt. %) of 38.1 mm diameter and 6 mm thickness. The discs were grit blasted and cleaned with acetone prior to spray.

Table 1 – HVOAF flame power and gases flowrates.

HVOAF setup	**Power (kW)**	**O_2 (%)**	**H_2 (%)**	**Air (%)**
HP – High power	48	25	59	16
MP – Medium power	41	23	49	28
LP – Low power	34	7	35	58

2.3 - Material characterisation

X-Rays diffraction (XRD) was carried out using a D8 Advance Da Vinci diffractometer (Bruker, Germany) with Cu cathode (k_α wavelength λ = 1.5406 Å) and θ-2θ Bragg-Brentano geometry. The diffractograms were acquired in the angular range 20° < 2θ < 70° at 0.02° steps with 0.2 s dwell time. The peak matching analysis has been carried out using Match! software (Crystal Impact, Germany). The carbide retention index (CRI) was calculated after background subtraction according to [23] by using Equation 1:

$$CRI = \frac{I_{WC}}{I_{WC}+I_{W_2C}+I_W} \quad (1)$$

with the intensity *I* of the peaks corresponding to WC, W_2C and W measured at the positions 2θ = 35.7°, 2θ = 39.8° and 2θ = 40.5°.

Journal Pre-proof

The scanning electron microscopy (SEM) characterisation of the coatings was carried out using an XL30 SEM (Philips, The Netherlands) for the top surfaces, cross-sections and wear tracks and a 7100F FEG-SEM (JEOL, Japan) for the WC-Co/CNT powder, in order to resolve the finely dispersed CNTs. Cross-sections were prepared by SiC disc cutting and hot mounting in conductive resin, ground using diamond (P900) and SiC (P1200) pads and polished using 6 µm and 1 µm diamond pads. Microhardness measurements were carried out on the cross-sections of the coatings using a Vickers microhardness indenter (Buehler, USA) by averaging the values from 10 indents made at the centre of the polished cross-section of the coatings, with a load of 300 gf and a dwell time of 10 s. Fracture toughness measurements (k_c) were carried out again on the cross-sections of the coatings using a Vickers microhardness indenter (Vickers instruments, United Kingdom) according to the Evans and Wilshaw method [24] according to Equation (2):

$$k_c = 0.079\left(\frac{P}{a^{\frac{3}{2}}}\right)\log\left(4.5\frac{a}{c}\right) \quad (2)$$

where P is the load, c is the crack length and a is the indent half diagonal. The results were obtained by averaging values from 5 indents made at the centre of the coatings, with a load of 5000 gf and a dwell time of 10 s. All the indents and cracks respected the applicability rule 0.6 < c/a < 5. The porosity was measured by area fraction using ImageJ on optical microscopy images of the cross-sections of the coatings, as they offered better contrast than SEM images avoiding confusion with dark phases. A threshold was chosen to separate the dark phase area A_{dp} corresponding to the porosity, with the remainder area, with the resulting porosity being $A_{por} = A_{dp}/A_{tot}$. To this end, three areas of interest of $A_{tot} = (200x200)\ \mu m^2$ were used for each sample and the results averaged. Raman spectroscopy measurements were carried out to analyse survival and structural integrity of CNTs. The instrument used is a LabRAM Raman microscope (Horiba Jobin Yvon, Japan) equipped with a 532 nm laser at 0.3 mW power. A confocal pinhole of 500 µm and a diffraction grating of 300 lines/mm were used.

2.4 - Wear tests

Wear tests were carried out using a Ball-on-disc tribometer (Ducom Instruments, The Netherlands) against a 6 mm diameter WC-Co counterbody ball (Dejay, United Kingdom)

with nominal surface roughness R_a = 0.04 µm. The WC-Co ball nominal composition is WC – 6 wt. % Co and its nominal hardness is 91 HRA which is equivalent to 1490 HV10. The top surface of the coatings was prepared for wear tests with the same grinding and polishing procedure used for cross-sections. All the tests were carried out at the same experimental conditions: 60 N load, 10 mm track diameter, 200 rpm angular speed (0.1 m/s linear speed at the contact point), for a total sliding distance of 2000 m. The wear tracks depth profile was measured using a Talysurf contact profilometer (Taylor Hobson, United Kingdom): 8 traverse profiles across the wear track equally distanced throughout the wear circumference were measured, averaged and multiplied with the wear track length to calculate the volume wear loss. The counterbody volume loss ΔV was calculated geometrically assuming the removal from a ball of radius r of a spherical cap of depth d, whose cap base a was measured by optical microscopy, according to Equations 3 and 4 [25]:

$$d = r - \sqrt{r^2 - a^2} \quad (3)$$

$$\Delta V = \pi d^2 \left(r - \frac{d}{3}\right) \quad (4)$$

The wear mass loss of both coating and counterbody ball was measured using a precision scale with 5 significant figures, and specific wear rates were calculated by accounting for load and total distance. The specific wear rate was then calculated by dividing volume and mass loss by the applied load and wear test distance.

3 – Results and discussion

3.1 - CNT incorporation on WC-Co powder

The sonication process of the WC-Co and CNT mixture in water had a dual effect in breaking the CNT agglomerates and allowing mixing of the WC-Co particles, which over time came in contact with the CNT. The outcome of the process is presented in Figure 1, where FEG-SEM images of the WC-Co/CNT particles are shown. In Figure 1a the WC-Co/CNT particles are visible at low magnification, where the WC and the Co binder phase can be seen in the typical hollow spheroidal shape. The CNTs, not evident at low magnification, can be seen in the high magnification image of Figure 1b. Here, these appear as small, scattered fibres nicely dispersed all over the WC-Co surface, with a very high concentration in some areas such as in the bottom left of the image. The lightweight and high surface to volume ratio of

the CNTs offers an effective van der Waals attraction which keeps them attached throughout the process from drying up to the spray stage. The outcome of this process is a hybrid powder that includes both the WC-Co and CNT materials and is readily usable as a powder feedstock for thermal spray, with controlled WC-Co to CNT ratio and little reduction in flowability. This novel process has the benefit of being relatively fast and scalable compared to existing CNT incorporation processes for thermal spray [26], opening the way for the production of large batches of readily usable nano-enabled powder.

Figure 1: Powder feedstock imaging – FEG-SEM images of WC-Co/CNT powder at low (a) and high (b) magnification. The typical hollow WC-Co particles composed of WC grains held together by the Co binder are shown, with the added CNT adhering to their surface. The CNTs are dispersed throughout the particles with varying density from sparse (black arrow) to dense (white arrow).

3.2 – Cross-sections and mechanical properties characterisation

The polished cross-sections of the coatings in SEM SE image are presented in Figure 2. The deposited thickness per pass was previously measured and found to decrease with decreasing flame power, from 12.5 µm for HP, to 10.5 µm for MP and 9 µm for LP, with no difference with or without CNT. All coatings show a well-bonded interface between the coating and the substrate with no interfacial porosity. The porosity within the coatings is reported in Table 2, with very low values (< 1%) in all the coatings except in the HP WC-Co case, where porosity is higher than 4%. Different flame powers appear not to affect the level of porosity globally; however, the 4% porosity case happens to be at high power, where the flame temperature is higher. Overall, the presence of CNTs, which ensures better heat dissipation, and lower power, which lowers the flame temperature, help keep the coating temperature lower during deposition and then hinder the formation of porosity.

Figure 2 – Low magnification coatings cross-sections - SEM BSE images of the cross-sections of the coatings obtained in high, medium and low power, with and without CNT. A compact morphology with limited porosity is shown, with a porosity-free coating/substrate interface.

The varying thickness arises from a varying number of passes when depositing the different coatings.

Table 2 – Coatings porosity measurements.

Porosity	**WC-Co**	**WC-Co/CNT**
HP – High power	(4.4 ± 0.5) %	(0.8 ± 0.4) %
MP – Medium power	(0.6 ± 0.2) %	(0.8 ± 0.2) %
LP – Low power	(0.8 ± 0.1) %	(0.8 ± 0.1) %

The high magnification microstructure of the coatings is shown in the SEM BSE images in Figure 3. Here it is possible to observe the typical WC-Co microstructure, with WC particles (bright phase) embedded in a Co binder matrix (grey phase). The porosity appears as black whereas additional features characterised by a higher atomic mass density, such as elemental W or W_2C phases, appear as the brightest phase; these can be seen at the WC/Co interface at the outer edge of the WC particles, as marked by circles in both MP images and in the HP WC-Co image. These features are most likely present in the coatings obtained at all powers, with a different frequency from one coating to another, as they are a by-product of the high temperature spray process itself. One additional interesting feature that occurs upon spray is the WC particles size refinement, of which one clear example is marked by the square in MP WC-Co where a cracked WC grain is shown. This does not compromise the quality of the coatings and can be conversely beneficial for their performance [27]. CNTs are not visible in these images as they are below the resolution threshold for SEMs in cross-section, and furthermore, the cross-section sample preparation is too aggressive for these nanoparticles.

Figure 3 – High magnification coatings cross-sections – SEM BSE images of the cross-sections of the coatings showing the typical WC-Co morphology with WC grains embedded in a Co matrix, identifiable thanks to Z contrast. Some features are highlighted such as WC decarburisation upon spray as shown by the brighter boundaries of the WC grains in the circles, and cracking of the WC grains upon spray as shown by the grain in the square.

The effect of CNTs on coatings microhardness is, however, evident, as shown in Figure 4a, where a net increase in microhardness both in the HP and in the LP case is associated with the presence of CNT. On the other hand, in the MP case it is the WC-Co coating which has the highest microhardness, even if the difference is very small, reaching the highest microhardness of all the coatings of about 1300HV. As the power is decreased, the WC-Co/CNT coatings show a slow descending trend in the hardness values, whereas no trend is identifiable in the WC-Co case. Concerning fracture toughness, the results are shown in Figure 4b, showing a general fracture toughness reduction when CNTs are added. This has been reported in the literature [28] as the CNTs themselves can be seeds for formation and propagation of cracks, thus decreasing the toughness of the material they are added to. Similarly to microhardness, a general descending trend is seen for the fracture toughness of the coatings containing CNTs as the power is decreased, possibly suggesting a less compact coating. If WC/Co samples are considered, again no trend is identifiable and the highest fracture toughness is found in the MP case; however, comparable within the error with the HP case, around 8 MPa·$m^{1/2}$. Note that the coatings were deposited using a different number of passes, therefore the resulting difference in thickness as evident in Figure 2. The comparison of their mechanical properties is, however, reliable as their thickness is always higher than 150 µm, which is much larger than the size of the indents, hindering the contribution from the substrate or the embedding resin.

Figure 4 - Coatings Vickers microhardness (a) and Fracture toughness (b) of the coatings.

A comparison of the mechanical and microstructural properties of the coatings in this work with results reported for coatings obtained with HVOF of similar powders confirms that the best performing coatings here reported are positioned around the high-end specification for microhardness, fracture toughness and porosity [29-31], notwithstanding the miniaturised gun for narrow apertures and very short stand-off distance.

3.3 – XRD phase characterisation and carbide retention

Journal Pre-proof

XRD was performed on the WC-Co powder and on the coatings to study phase changes and decarburisation. The by-products of decarburisation are the W_2C and elemental W phases, which are undesirable as they can worsen the performance of the coating [32]. The XRD spectra are shown in Figure 5a, where all the different phases found are marked. The WC-Co powder spectrum shows the two expected sets of WC and Co peaks and a faint amorphous region around 2θ = 30°. In all the spectra of the coatings, the WC peaks are still present, but the Co peaks disappear. This is due to the melting of the crystalline Co into the amorphous matrix that binds the WC particles together in forming the coating. Minor dissolution of C and W in the Co matrix in forming Co6W6C yielded the partially amorphous region centred at 2θ = 43°, which has more crystalline character in LP. Additional peaks appear upon spray in the spectra of the coatings, namely those corresponding to W_2C and W phases: these peaks appear since WC decarburised due to the high temperature of the spray process. Consequently, these peaks are more pronounced at high power and are instead very weak or non-identifiable at lower power. Quantitatively, the carbide retention index was calculated and is presented in Figure 5b. The high power case is the clearer one, with very minor carbide loss upon spray, while in the medium power case there is a mixed result depending on the presence of the GNP. Overall, the effect of decreasing the power, thus lowering the process temperature, is that of lowering amorphisation and decarburisation. In order to assess the effect of the presence of CNT on decarburisation, the interesting case is in fact the medium power, where W_2C and W peaks are visibly more pronounced in the WC-Co case compared to the WC-Co/CNT case. The carbide retention index increases in fact from around 0.88 up to almost 0.95. This finding suggests that the presence of CNTs has a similar effect to that of decreasing the power and keeping the process temperature low, possibly by helping to keep the coating temperature low thanks to their high thermal conductivity. At the same time, the presence of CNT has a negligible effect in the extreme cases of low and high power, where the power itself has a significant effect in determining the retention of carbides.

Figure 5 – a) X-rays diffraction – XRD of the powder and coatings. The powder shows typical WC and Co phases. The coatings show an amorphous hump originated from minor W and C dissolution in the Co matrix, showing the increasingly amorphous character as the flame

power increases. Evidence of decarburisation is shown in high and medium power as two main additional peaks from W_2C and W appear at around 40°. b) Carbide retention index calculated for the different coatings based on the WC, W_2C and W XRD peak intensities according to the method in [23].

3.4 – Raman spectroscopy and CNT degradation

The low concentration of CNTs (0.5 wt. %) makes them non-detectable with XRD, where normally only phases above 2 wt. % can be properly identified. A more efficient way of detecting and studying CNTs is Raman spectroscopy. A Raman spectrum from the as received CNT powder is presented in Figure 6a, showing the D, G and 2D bands which are typical of carbon allotropes, and an additional higher-order D+D' band. The relative change in height and shape of these bands yields information on the structural degradation CNTs may have undergone [33], in particular within the single tube wall (D band) or between the different tube walls (2D) [34], in analogy with graphene layers stacking [35]. An increase of the intensity of the D band compared to the G band, and a decrease of the intensity and broadening of the 2D band would suggest structural degradation has occurred: substitutional atoms, vacancies, lattice distortions or stacking faults. When comparing the as-received CNT spectrum with the spectra from randomly chosen areas containing CNT from HP, MP and LP coatings, in Figures 6b, 6c and 6d, it emerges how the relative height and shape of the bands is very similar in all the spectra, with minimal differences attributable to the particular CNT-containing area of choice, indicating no or minor degradation has happened as a result of feedstock preparation and thermal spray deposition. The short interaction time between the feedstock and the thermal spray combustion flame, of the order of milliseconds, prevents any major spray-induced degradation, as reported from previous works involving carbon allotropes [18, 36]. Furthermore, WC-Co powder has been shown to act as a carrier and to provide thermal shielding to CNTs when sprayed using HVOF, plasma spray and cold spray [37], and is confirmed in this work for HVOAF in ID configuration.

Figure 6 – Raman spectroscopy – Raman spectra of the CNT as-received powder and of the CNT present in the coatings obtained at the three power conditions. All the spectra show

very similar features with the main D, G and 2D bands typical of graphitic structures. The relative height of the bands is similar for all spectra indicating than no major CNT degradation has occurred upon spray.

3.5 – Wear performance

Wear tests were carried out on the coatings to assess their wear resistance and friction properties. The specific wear rates in terms of volume and mass are presented in Figure 7a for the coating and 7b for the counterbody. The presented results are averages from two repeated tests, with standard error used as associated uncertainty. All the trends from the mass measurements agree with the volume measurements, validating the relevance of the results. Concerning the coating, interesting trends emerge from Figure 7a, where all the coatings containing CNT appear to have a higher specific wear rate than their WC-Co only counterparts, by approximately a factor 2. As the power changes, it can be noticed how HP and MP perform similarly, with slightly lower specific wear rate for MP, whereas LP presents higher specific wear rate, of approximately a factor 2 compared to HP and MP, which results from the overall lower microhardness as presented in Figure 4.

A different picture emerges from the counter body specific wear rate in Figure 7b. Here, the presence of CNT is associated with a significant reduction of specific wear rate in HP, whereas a slight increase is seen in MP and LP, in line with the coating behaviour. Concerning the power, a general decreasing trend in the specific wear rate is seen as the power decreases, with LP presenting the lowest counter body specific wear rate for both WC-Co and WC-Co/CNT. The HP high specific wear rate in the WC-Co case can be explained by the much higher porosity presented by this coating as in Table 2, which can favour a more abrasive wear behaviour, particularly detrimental for the counter body. Considering the combined coating and counter body specific wear rate, MP WC-Co is the coating providing the most efficient wear resistance in these test conditions. A comparison with a similar work [14], noteworthy thanks to the small differences in the spray setup and feedstock chosen, suggests that similar or lower values of specific wear rate are achieved in our work possibly. In their case, the addition of CNT improved the wear rate due to an improvement of the microhardness and fracture toughness of the coatings; however, in our case the addition of CNT does not improve the specific wear rate since the microhardness is enhanced but the fracture toughness is not. At the same time, our microhardness and

fracture toughness values are generally very high, ensuring a very low wear rate for all coatings, with and without CNTs.

Figure 7 – Wear tests - wear rate – Specific wear rate of the coating (a) and of the counterbody (b) where the blue histograms indicate the volume loss (left y axis) and the orange dots indicate the mass loss (right y axis). The values are obtained by averaging two tests and the associated error is the standard error.

Additional insight into the wear tests is provided by the friction information, presented in Figure 8. Figure 8a shows the coefficient of friction over distance for the various coatings. It is noticeable how both HP coatings present an unstable behaviour, with sudden changes in coefficient of friction, whereas all the others show smoothly varying coefficient of friction curves. There is also, in general, a bedding in spike, except for the HP WC-Co coating. The atypical behaviour of the HP coating can be attributed to its high porosity. Regarding the quantification of the coefficient of friction for comparison, as suggested by steady-state values and supported by average values in Figure 8b, MP WC-Co coating offers the lowest coefficient of friction of all. Among the coatings with CNT, HP WC-Co/CNT is offering the lowest average value, and an increasing trend can be identified as the power goes from HP to LP. The effect of the addition of CNT on the coefficient of friction is negligible within the errors in LP condition, causes an approximate 50% increase in MP and a 50% decrease in HP condition.

Figure 8 – Wear tests – Coefficient of friction – (a) Coefficient of friction as a function of distance of the first wear test and (b) coefficient of friction averaged over the whole distance of the two tests with standard deviation as associated uncertainty.

SEM images of the wear tracks provide a deeper insight in the wear behaviour. The HP coatings are shown in Figure 9. A similar surface preparation was undertaken for all samples which may lead to some variation of residual surface roughness at the beginning of the wear tests, which can have an effect on the initial wear cycles but will yield negligible effects on the wear test as a whole. A comparison of the low magnification SE images in Figure 9a and 9b shows how the WC-Co/CNT wear track is more pronounced and contains a higher

amount of debris than the WC-Co. These features suggest a three-body wear has occurred in this case, which has the dual effect of lowering the coefficient of friction while causing abrasive wear and then a higher wear rate, as confirmed by previous analyses. From the high magnification BSE images in Figure 9c and 9d, cracked oxidised patches are visible in both coatings, while some pores are visible in WC-Co only, which are likely to be due to the initial high porosity instead of grain pull-outs. The WC-Co/CNT coating on the other hand shows signs of ploughing, as a result of the three-body abrasive wear.

Figure 9 – Wear track imaging of coatings sprayed at high power - SEM BSE images of the wear tracks of the HP (a, c) and HP CNT (b, d) coatings. The main features presented include debris in (b) and oxidised patches in (c) and (d) where signs of cracking and ploughing (horizontal marks indicated by the arrows) are present.

Considering now the MP coatings presented in Figure 10, it is again possible to detect a more evident wear track in WC-Co/CNT compared to the WC-Co case, where only a very faint mark is visible. As a support to this, in Figure 10c it is shown only an early onset of oxidation whereas in 10d extended oxidised patches with cracks are visible. Abrasive wear is here not evident, as little debris is present and no ploughing marks can be found.

Figure 10 – Wear track imaging of coatings sprayed at medium power - SEM BSE images of the wear tracks of the MP (a, c) and MP CNT (b, d) coatings. A very faint wear track is shown in (a) with corresponding small oxidised patches and limited cracks in (c). Conversely, a higher amount of oxidised patches along with signs of ploughing and cracks are shown in (d).

The LP coatings shown in Figure 11 offer a very different picture. The wear tracks in Figure 11a and 11b are both very evident, and also narrower compared to the previous coatings obtained in HP and MP conditions. Here, the coating is wearing to a great extent compared to the ball, leading to a deep and narrow track, as confirmed by the previous wear rate analyses. The BSE images in Figure 11c and 11d both show a high amount of oxidation and cracking, in line with the higher amount of wear occurred and higher than all the coatings analysed so far. Some debris is present though not as much as in HP WC-Co/CNT case, however, ploughing marks can be easily seen as a higher fraction of the wear track has here

transformed into the softer oxidised patches, more subject to ploughing marks.
An SEM-EDX characterisation, not shown here, of an oxidised patch from the wear track of sample HP WC-Co chosen as an example, has revealed both Co and W oxides are present and therefore form upon wear testing. Tribo-oxidation of both Co and W is therefore one of the mechanisms of wear.

Figure 11 – Wear track imaging of coatings sprayed at low power - SEM BSE images of the wear tracks of the LP (a, c) and LP CNT (b, d) coatings. Narrow but clearly visible wear tracks are shown in (a, b) with corresponding extensive oxidised patches in (c, d). Large cracks appear in particular in (c).

3.6 - Effect of flame power and CNT addition

The change in flame power yields several noticeable effects in the coatings and their performance, although it is not always possible to detect a monotone trend in the properties of the coatings as the power changes. As reported in Table 1, in the low power case the air flowrate is much higher than in the other cases and the flow rate of oxygen is the lowest. A comparison between low and medium flowrate is more complex as the two combination of gases have a similar oxygen proportion, where in the medium flowrate the additional air counterbalances the lower flow rate of oxygen and hydrogen. As a general trend, a lower power yields lower microhardness and fracture toughness, lower decarburisation, higher coating specific wear rate, lower counter body specific wear rate and a higher degree of oxidation in the worn surface. Considering wear resistance, the MP WC-Co coating shows a collection of the most desirable properties: the lowest porosity, the highest microhardness and fracture toughness, lowest specific wear rate, lowest coefficient of friction and a wear track with little oxidation and debris. On the other hand, it is characterised by decarburisation to the greatest extent among all coatings here presented, but this does not compromise the performance of the coating. If the mating surface was to be protected instead of the coating itself, here it is the LP WC-Co coating showing the lowest counter body specific wear rate. Its combined effect of relatively low microhardness and fracture toughness is playing the major role in this, as it favours the sacrificial wear of the coating itself instead.

The addition of CNT has shown a variety of effects on the structure, composition and tribomechanical properties of the coatings. CNT thermal conductivity has been reported in the 2800-6000 W/mK range [38-40], which is one order of magnitude higher than that reported for WC-Co (60-160 W/mK) [41,42]. The presence of CNT, thanks to their high thermal conductivity, enhances the thermal conductivity of the coatings, offering a better heat dissipation and ensuring a lower sample temperature during spray. This effect is highlighted by the lower porosity in the HP CNT case compared to the HP case, and especially by the lower amount of decarburisation detected by XRD in the MP CNT case compared to the MP case. This effect does not yield measurable improvements to the wear tests but can be relevant and beneficial in high temperature applications where heat depletion is needed.

Alongside, a clear increase in microhardness has been found in HP and LP conditions when CNTs are added. This effect has been found elsewhere and is expected due to the exceptional mechanical properties of CNT [16], which enhance those of the coating. An unexpected effect is that of medium power spray condition, where the microhardness does not improve with the addition of CNT and, conversely, slightly decreases. In this case the WC-Co microhardness is already very high, and the CNTs are not able to improve it further. The beneficial effects of adding CNTs to WC-Co emerge in the high power case where, in addition to the increase in microhardness, both counter body wear rate and coefficient of friction are substantially decreased, offering a favourable scenario if the mating surface has to be protected and if a low energy dissipation through friction in the form of heat is desirable.

It is worth noticing that wear performance, when adding CNTs, generally decreases in the other two cases: medium and low power. CNT are found here to generally decrease the fracture toughness of the coatings, as does lowering the power from high to low. The combined effect of these two parameters brings the fracture toughness of MP CNT and LP CNT below the threshold of 5 $MPa \cdot m^{1/2}$, leading to a poorer wear performance and therefore hiding any possible benefit of CNT addition to wear performance, which in fact emerges only in the HP CNT case. Overall, the coatings showing a higher fracture toughness are also those showing a better wear performance (lower specific wear rate). Since one of the main failure mechanisms is cracking, with following material removal and debris

formation, the coatings with higher fracture toughness are better at reducing this wear mechanism.

The three different flame power parameters also influence the CNTs in-flight. Even if CNTs are known to be able to survive thermal spray [14], as are other 2D materials both as nanocomposites [19] and alone [17], a certain amount of degradation should be foreseen due to the high temperature and oxygen presence in the flame. This degradation has not been detected in this work, where CNTs in the coatings showed pristine Raman spectra, but may be detected by a comparison of the concentration of CNT in the final coatings compared to the starting powders, which is beyond the scope of this work. The heat resistance of CNTs is remarkable even at high temperatures of thermal spray, especially due to their high thermal conductivity and strong covalent bonded structure. Regarding oxidation resistance, the HVOAF flame can be tuned to provide different stoichiometries of fuel to oxygen which in this work are around 2.1% for HP conditions and 1.7% for MP and LP. This yields a slightly reducing atmosphere for HP and oxidising atmosphere for MP and LP, which suggests an overall lower degradation of CNTs upon thermal spray and adds up to the explanation why HP coatings are the most benefited by the addition of CNTs. Another aspect that goes beyond the scope of his work is the change in CNT concentration. The addition of a higher concentration of CNT has been shown to improve the tribology and wear properties of CNT composites; this at the expense of microhardness, which in turn is reduced [43], and fracture toughness. Therefore, it is advisable to tailor the CNT concentration according to the aimed application and optimise tribological or mechanical properties.

Conclusion

WC-Co/CNT coatings have been deposited with HVOAF and the effect of changing spray parameters as well as the effect of CNT addition has been investigated.
CNTs were successfully incorporated using a novel setup in commercial WC-Co powder for thermal spray, undergoing no or minimal degradation upon ID-HVOAF thermal spray as confirmed by Raman spectroscopy. Low power and the presence of CNTs helps hinder decarburisation by keeping the process temperature lower and favouring heat dissipation. The HP conditions are the most benefited by the addition of CNT, with a reduction in coefficient of friction by half, an increase in microhardness and a decrease in porosity and

counter body wear rate. However, not all the samples benefited by the addition of CNT as the decrease in fracture toughness can disrupt wear performance.
The applicability of this process extends beyond the scope of this work offering a practical way to develop various combinations of commercial powders and nanofillers.

Acknowledgements

This work has been conducted in the framework of Innovate UK project "Nano-Reinforced Coatings with Improved Thermomechanical Properties - Steel Sector Application (UNICAST)" [Project No:104768] led by Monitor Coatings Ltd. This work was also supported by the Engineering and Physical Sciences Research Council [grant number EP/R511730/1]. The authors acknowledge the Nanoscale and Microscale Research Centre (nmRC) at the University of Nottingham for access to the SEM, FEG-SEM and Raman spectroscopy facilities.

CRediT author statement

Federico Venturi: Conceptualisation, Methodology, Investigation, Writing – original draft, Visualisation. **Spyros Kamnis:** Conceptualisation, Methodology, Writing - Review & Editing, Project administration. **Tanvir Hussain.** Validation, Resources, Writing - Review & Editing, Supervision.

Data availability

The raw data required to reproduce the findings of this work cannot be shared at this time as the data also forms part of an ongoing study.

Declaration of interests

The authors declare that they have no known competing financial interests or personal relationships that could have appeared to influence the work reported in this paper.

The authors declare the following financial interests/personal relationships which may be considered as potential competing interests:

Journal Pre-proof

References

[1] T. Hoornaert, Z. K. Hua, and J. H. Zhang (2009) *Hard Wear-Resistant Coatings: A Review*. In: Luo J., Meng Y., Shao T., Zhao Q. (eds) Advanced Tribology. Springer, Berlin, Heidelberg

[2] P. A. Sørensen, S. Kiil, K. Dam-Johansen, and C. E. Weinell, *Anticorrosive coatings: a review*, Journal of Coatings Technology and Research **6** (2009) pp 135–176.

[3] P. H. Shipway, I. M. Hutchings, *Measurement of coating durability by solid particle erosion,* Surface and Coatings Technology **71** (1995) pp 1–8.

[4] P. G. Lashmi, P. V. Ananthapadmanabhan, G. Unnikrishnan, and S. T. Aruna, *Present status and future prospects of plasma sprayed multilayered thermal barrier coating systems*, Journal of the European Ceramic Society **40** (2020) pp 2731-2745.

[5] D. Tejero-Martin, M. Rezvani Rad, A. McDonald, and T. Hussain, *Beyond Traditional Coatings: A Review on Thermal-Sprayed Functional and Smart Coatings*, Journal of Thermal Spray Technology **28** (2019) pp 598–644.

[6] L.-M. Berger, *Application of hardmetals as thermal spray coatings*, International Journal of Refractory Metals and Hard Materials **49** (2015) pp 350-364.

[7] C. Lyphout and S. Björklund, *Internal Diameter HVAF Spraying for Wear and Corrosion Applications*, Journal of Thermal Spray Technology **24** (2015) pp 235–243.

[8] W.-Y. Li and C.-J. Li, *Optimal design of a novel cold spray gun nozzle at a limited space*, Journal of Thermal Spray Technology **14** (2005) pp 391–396.

[9] J. Pulsford, F. Venturi, Z. Pala, S. Kamnis, and T. Hussain, *Application of HVOF WC-Co-Cr coatings on the internal surface of small cylinders: Effect of internal diameter on the wear resistance,* Wear **432-433** (2019) n 202965.

[10] S. E. Franklin and J. Beuger, *A comparison of the tribological behaviour of several wear-resistant coatings*, Surface and Coatings Technology **54-55** (1992) pp 459–465.

[11] A.S. Kurlov, A.I. Gusev, *Tungsten Carbides: Structure, Properties, and Application*. Springer, Switzerland; (2013) pp 1-3.

[12] R. Schwetzke and H. Kreye, *Microstructure and properties of tungsten carbide coatings sprayed with various high-velocity oxygen fuel spray systems*, Journal of Thermal Spray Technology **8** (1999) pp 433–439.

[13] H. Wang, Q. Qiu, M. Gee, C. Hou, X. Liu, X. Song, *Wear resistance enhancement of HVOF-sprayed WC-Co coating by complete densification of starting powder*, Materials & Design **191** (2020) n 108586.

Journal Pre-proof

[14] D. Mohanty, S. Kar, S. Paul, P. P. Bandyopadhyay, *Carbon nanotube reinforced HVOF sprayed WC-Co coating*, Materials & Design **156** (2018) pp 340–350.

[15] C. Lee, X. Wei, J. W. Kysar, and J. Hone, *Measurement of the Elastic Properties and Intrinsic Strength of Monolayer Graphene*, Science **321** (2008) pp 385-388.

[16] M.-F. Yu, O. Lourie, M. J. Dyer, K. Moloni, T. F. Kelly, and R. S. Ruoff, *Strength and Breaking Mechanism of Multiwalled Carbon Nanotubes Under Tensile Load*, Science **287** (2000) pp 637-640.

[17] F. Venturi, G. A. Rance, J. Thomas, and T. Hussain, *A low-friction graphene nanoplatelets film from suspension high velocity oxy-fuel thermal spray*, AIP Advances **9**, 025216 (2019) pp 1-6.

[18] J. W. Murray, G. A. Rance, F. Xu, and T. Hussain, *Alumina-graphene nanocomposite coatings fabricated by suspension high velocity oxy-fuel thermal spraying for ultra-low-wear*, Journal of European Ceramic Society **38** (2018) pp 1819-1828.

[19] F. Venturi, J. Pulsford, T. Hussain, *A novel approach to incorporate graphene nanoplatelets to Cr_2O_3 for low-wear coatings*, Materials Letters **276**, 128283 (2020) pp 1-4.

[20] W. X. Chen, J. P. Tu, L. Y. Wang, H. Y. Gan, Z. D. Xu, and X. B. Zhang, *Tribological application of carbon nanotubes in a metal-based composite coating and composites*, Carbon **41** (2003) pp 215-222.

[21] M. A. Rodríguez, L. Gil, S. Camero, N. Fréty, Y. Santana, J. Caro, *Effects of the dispersion time on the microstructure and wear resistance of WC/Co-CNTs HVOF sprayed coatings*, Surface and Coatings Technology **258** (2014) pp 38-48.

[22] B. Allcock, S. Gu, and S. Kamnis, US patent no 2017/0335441 A1

[23] C. Lyphout and K. Sato, *Screening design of hard metal feedstock powders for supersonic air fuel processing*, Surface and Coatings Technology **258** (2014) pp 447–457.

[24] A. G. Evans and T. R. Wilshaw, *Quasi-static solid particle damage in brittle solids-I. Observations, analysis and implications*, Acta Metallurgica **24** (1976) pp 939-956.

[25] P. Shipway, *The role of test conditions on the microabrasive wear behaviour of soda-lime glass*, Wear 233-235 (1999), pp 191-199.

[26] D. Kaewsai, A. Watcharapasorn, P. Singjai, S. Wirojanupatump, P. Niranatlumpong, S. Jiansirisomboon, *Thermal sprayed stainless steel/carbon nanotube composite coatings*, Surface and Coatings Technology **205** (2010), pp 2104-2112.

[27] Q. Yang, T. Senda, and A. Ohmori, *Effect of carbide grain size on microstructure and sliding wear behavior of HVOF-sprayed WC-12% Co coatings*, Wear **254** (2003) pp 23–34.

Journal Pre-proof

[28] B. Yazdani, Y. Xia, I. Ahmad, and Y. Zhua, *Graphene and carbon nanotube (GNT)-reinforced alumina nanocomposites*, Journal of the European Ceramic Society **35** (2015) pp 179–186.

[29] V. Katranidis, S. Gu, B. Allcock, S. Kamnis, *Experimental study of high velocity oxy-fuel sprayed WC-17Co coatingsapplied on complex geometries. Part A: Influence of kinematic sprayparameters on thickness, porosity, residual stresses and microhardness*, Surface and Coatings Technology **311** (2017) pp 206–215.

[30] T. Y. Cho, J. H. Yoon, K. S. Kim, K. O. Song, Y. K. Joo, W. Fang, S. H. Zhang, S. J. Youn, H. G. Chun, S. Y. Hwang, *A study on HVOF coatings of micron and nano WC–Co powders*, Surface and Coatings Technology **202** (2008) pp 5556–5559.

[31] S. M. Nahvi, M. Jafari, *Microstructural and mechanical properties of advanced HVOF-sprayed WC-based cermet coatings*, Surface and Coatings Technology **286** (2016) pp 95–102.

[32] C. J. Li and G. J. Yang, *Relationships between feedstock structure, particle parameter, coating deposition, microstructure and properties for thermally sprayed conventional and nanostructured WC-Co*, International Journal of Refractory Metallic Hard Materials **39** (2013) pp 2–17.

[33] B. Capaz, M. V. O. Moutinho, A. Lombardo, T. S. Kulmala, and A. C. Ferrari, *Quantifying Defects in Graphene via Raman Spectroscopy at Different Excitation Energies*, Nano Lett. **11** (2011) pp 3190-96.

[34] M. S. Dresselhaus, A. Jorio, M. Hofmann, G. Dresselhaus, and R. Saito, *Perspectives on Carbon Nanotubes and Graphene Raman Spectroscopy*, Nano Lett. **10** (2010) pp 751-758.

[35] L. M. Malard, M. A. Pimenta, G. Dresselhaus, and M. S. Dresselhaus, *Raman spectroscopy in graphene*, Phys. Rep. **473** (2009) pp 51-87.

[36] F. Venturi and T. Hussain, *Radial injection in Suspension High Velocity Oxy-Fuel (S-HVOF) thermal spray of graphene nanoplatelets for tribology*, Journal of Thermal Spray Technology **29** (2019) pp 255-269.

[37] A. K. Keshri, K. Balani, S. R. Bakshi, V. Singh, T. Laha, S. Seal, A. Agarwal, Structural transformations in carbon nanotubes during thermal spray processing, Surface and Coatings Technology **203** (2009) pp 2193-2201.

[38] C. Yu, L. Shi, Z. Yao, D. Li, and A. Majumdar, *Thermal conductance and thermopower of an individual single-wall carbon nanotube*, Nano Letters **5** (2005) pp 1842–1846.

[39] P. Kim, L. Shi, A. Majumdar, and P. L. McEuen, *Thermal transport measurements of individual multiwalled nanotubes,* Phys Rev Lett **87** (2001) n 215502.

[40] J. E. Fischer, *Carbon nanotubes: structure and properties*. In: Y. Gogotsi ed. Carbon nanomaterials. New York: Taylor and Francis Group; (2006) pp 51–58.

Journal Pre-proof

[41] W. S. Williams, *The thermal conductivity of metallic ceramics, JOM* **50** (1998) pp 62–66.

[42] M. V. Frandsen and W. S. Williams, *Thermal Conductivity and Electrical Resistivity of Cemented Transition-Metal Carbides at Low Temperatures*, Journal of American Ceramic Society **74** (1991) pp 1411-1416.

[43] A. Kasperski, A. Weibel, D. Alkattan, C. Estournès, V. Turq, C. Laurent, and A. Peigney, *Microhardness and friction coefficient of multi-walled carbon nanotube-yttria-stabilized ZrO2 composites prepared by spark plasma sintering*, Scripta Materialia **69** (2013) pp 338–341.

Graphical abstract

Highlights

- A novel setup was developed to incorporate carbon nanotubes in commercial WC-Co powder for thermal spray.
- As confirmed by Raman spectroscopy, carbon nanotubes undergo no or minimal degradation upon internal diameter high velocity oxy-air-fuel thermal spray.
- Decarburisation upon spray is reduced by low power (lower process temperature) and the presence of carbon nanotubes (better heat dissipation).
- In high power conditions, carbon nanotubes halve coefficient of friction, increase microhardness and reduce porosity and counterbody wear rate.

Journal Pre-proof